Applied Cardiopulmonary Pathophysiology 21: 3-17, 2017

In Silico Simulations Compared to *In Vivo* Measurements of the Effects of Fluid Properties on Dynamic Ventilation Parameters during Xenon Anesthesia

Ira Katz[1,2], Caroline Majoral[1], Christian Daviet[1], Jean-Etienne Bazin[3], Georges Caillibotte[1]

[1] Medical R&D, Air Liquide Santé International, Centre de Recherche Claude-Delorme, 78354, Jouy-en-Josas, France; [2] Department of Mechanical Engineering, Lafayette College, Easton, PA, 18042, USA; [3] Service d'Anesthésie-Réanimation, CHU Estaing, 1 place Lucie Aubrac, 63003 Clermont-Ferrand

Abstract

In this paper *in vivo* measurements and the results of an *in silico* analysis of the effects of fluid property variation on dynamic ventilation parameters during xenon anesthesia are presented. The *in vivo* measurements of dynamic ventilatory parameters were taken prior to surgery during the wash-in phase of xenon anesthesia. The in *silico* model is based on a quasi-static time integration of an engineering pressure loss approach to simulate dynamic respiratory parameters during volume control mode mechanical ventiliation. The in *silico* model is shown to compare well with the measurements and used to directly compare the effects of fluid properties of three gas mixtures on the ventilatory parameters of peak minus plateau pressure and the maximum expiratory flow rate. Thus the use of physics based models to inform physicians of the impact of administering gas mixtures seems feasible.

Keywords: lung, morphology, numerical modeling, supine, ventilator

Introduction

The variation of ventilatory parameters of flow rate and airway pressure loss (often combined to form the airway resistance) that depend on a myriad of subject specific variables are fundamental to understand the mechanics of breathing, either spontaneously or via mechanical ventilation as described in classic papers by Otis and colleagues (1) and to the present day (2). Of particular interest is airway resistance related to respiratory disease (3–5) and to safe mechanical ventilation (6,7). With this interest in respiratory fundamentals there has been considerable effort in the development of models based on analytical (6,8,9), experimental (10,2), and computational fluid dynamics (11,12) approaches to study the phenomena and to extend the understanding by investigating physiological parameters that are difficult or impossible to accomplish *in vivo*. For example, the pressure distribution through the airways to the alveoli can be readily calculated but not directly measured.

In previous papers a relatively simple analytical *in silico* model, the engineering pressure loss model, for airways has been introduced and applied to the ventilation distribution as a function of inertial flow losses (8), the airway pressure distribution during xenon anesthesia (13), and the pressure dis-

tributions for medical gas mixtures calculated in an infant airway morphology model (14). Furthermore, this model was validated in an *in vitro* study as reported in the literature. (2) The aim of the current study is to validate the use of the model using *in vivo* data and specifically to assess the capabilities of the model to account for different gas property values and the dynamics of the respiratory cycle. This is accomplished via comparisons with dynamic *in vivo* measurements that show that the model is capable of replicating the ventilation parameters as measured by a ventilator in volume control mode during the wash-in phase of xenon anesthesia.

Methods

Ethics

This physiological-pharmacological, observational, prospective non-randomised, investigator sponsored study was approved by the ethics committee French CPP Sud-Est 6 (IRB N° IRB00008526). A total of 10 male (6) and female (4) patients aged between 50 and 83, ASA 1 or 2 without history of respiratory disease scheduled for an abdominal surgery under xenon anaesthesia were enrolled in the study (see Table 1 for patient characteristics). The nature of the study was explained to the subjects and each one signed an informed consent form.

Measurements

Patients were installed in the supine position with the standard monitoring (electrocardioscope, non invasive blood pressure, saturation of peripheral oxygen (SpO_2), Bi-spectral Index (BIS)) put in place. Anaesthesia was induced with propofol and remifentanil administered with a target controlled technique (Base Primea Fresenius, France). Each patient's trachea was intubated with a size 7.5 or 8 mm Edgar type endotracheal tube (ETT) (Rusch, Ireland). The patients were ventilated using volume controlled mode with a tidal volume (V_T) between 8 and 10 mL/kg of theoretical ideal body weight and a frequency of 10 breaths per minute using a FELIX DUAL anaesthetic ventilator station (Air Liquide Medical Systems, France). The FELIX DUAL was specifically designed for xenon anaesthesia including flow calibration, xenon gas concentration, and a mode for economising gas usage.(15,16) If necessary, the V_T was secondarily adapted in order to maintain end tidal partial pressure of carbon dioxide ($PetCO_2$) between 35 and 40 mmHg,

Table 1: Patient characteristics. NA is not available. Only two values are used for the average compliance of P#3.

P#	Sex	Age	BMI	ETT size (mm)	Average Compliance (ml/cm H2O)	Compliance StdDev
1	F	68	27.7	7.5	NA	NA
2	M	59	24.2	8	57.5	8.1
3	M	74	34.9	7.5	38.8	1.7
4	M	66	24.7	7.5	48.1	7.2
5	F	70	23.9	7.5	37.1	7.4
6	F	74	25.5	7.5	39.9	4.1
7	F	56	30.5	7.5	44.2	7.1
8	M	72	27.0	8	60.1	8.3
9	M	50	25.4	8	48.7	1.6
10	M	83	26.0	8	55.6	11.2

with an inspiratory/expiratory (I:E) ratio of 1:2. A positive end expiratory pressure (PEEP) of nominally 5 to 10 cmH_2O was applied during the entire anaesthesia.

After endotracheal intubation and stabilisation, 100% oxygen was delivered for 10 minutes (that also allowed for partial denitrogenation of the tissues) before a first set of measurements were recorded for approximately three breathing cycles (T1). Xenon (LENOXe, Air Liquide Santé International, France) was then introduced into the ventilatory circuit with an ultimate target of inhaled concentration of 60%. When the xenon concentration was between 28 and 32% a second data recording for three breathing cycles was made (T2a). After 5 minutes of stabilisation at 60% xenon the third recording of data of similar length was performed (T2). During the progressive increase of xenon concentration the target concentration of propofol was progressively decreased in order to maintain the bispectral index values between 40 and 50. In case of laparoscopic surgery (7 patients), a recording of data was realised 5 minutes after the inflation of pneumoperitoneum (T2b). At the end of the surgical procedure, after deflation of pneumoperitoneum in case of laparoscopy, a last recording during three breathing cycles was realised with a xenon concentration of 60% just before the end of administration of the gas (T3). The data from the wash-in phase, measurement points T1, T2a, and T2, will be presented. Figure 1 is a schematic of the timing for the data recording. In effect, this protocol provided three test gas mixtures with different densities and viscosities.

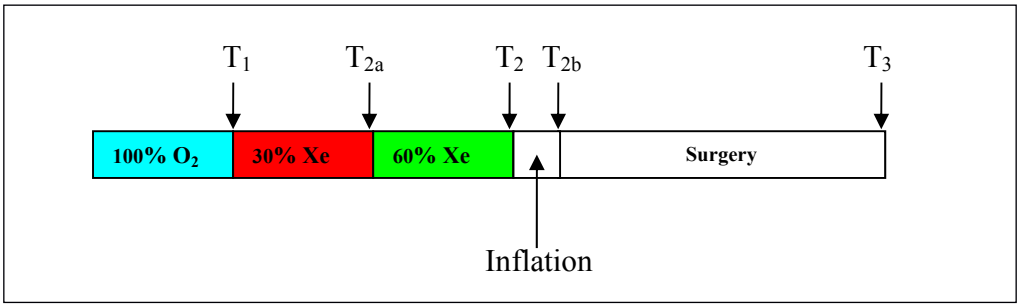

Figure 1: Schematic of timing of data recording.

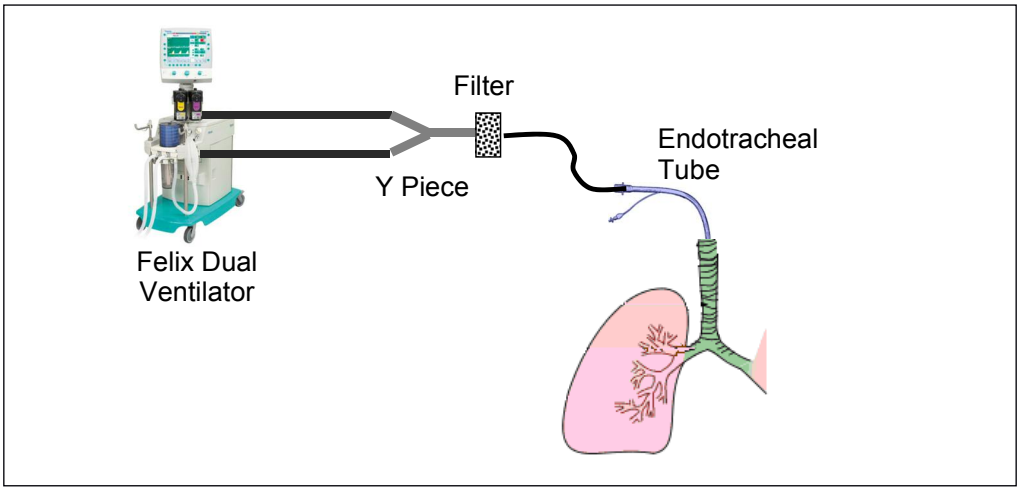

Figure 2: Schematic of the ventilator circuit and respiratory tract.

Ventilation and respiratory data monitoring of flow rate, pressure at the Y-piece of the patient circuit (see Figure 2 for a schematic), inhaled and expired volume, and concentration of oxygen, xenon, and carbon dioxide were recorded on the anaesthesia station and downloaded to a portable computer at a rate of 20 Hz (50 ms intervals). All these measurements were purely observational, realised without modification of the ventilation or any other intervention on the patients. The recorded resolution of the digital pressure and flow measurements were 1 cm H_2O and 1 l/min, respectively. The resolution of inhaled volume, based on the time integration of the flow signal, was 1 ml. The relevant variables for this study were found for each patient by analyzing one of the downloaded waveforms for each gas mixture (V_T, respiratory rate (RR), PEEP, peak pressure during inhalation (p_{peak}), plateau pressure ($p_{plateau}$), inhalation flow rate (Q_{in}), and the maximum exhalation flow rate ($Q_{max\text{-}ex}$)). The lung compliance (C) was calculated based on $C = V_T/(p_{plateau}\text{-PEEP})$ for each gas mixture and averaged for use in calculations (provided in Table 1). Airway resistance for inhalation was calculated using $R_{AW} = Q_{in} / (p_{peak} - p_{plateau})$. However, this is not a true airway resistance because it includes the breathing circuit from the Y-piece through the ETT to the trachea, bypassing the upper airways.

The number of patients was arbitrarily fixed to 10.

In Silico Model

The *in silico* analytical model is described in detail in a previous paper. (8) Briefly, for a constant insufflation flow rate, the pressure at any location in the respiratory tract compared to the alveolar pressure is

$$p - p_{alv} = \rho \sum h - \rho \left(\alpha \frac{V^2}{2} \right) \quad , \qquad (1)$$

where p and V are the pressure and average velocity at each location, ρ is the gas density, and α is a coefficient that modifies the kinetic energy term to account for different flow profiles: $\alpha = 1$ for a blunt velocity profile and 2 for a parabolic profile. The summation on the right-hand-side of Equation 1 is called the head loss, which represents the sum of all the resistive energy losses per unit mass in the flow path.

In this typical engineering approach, the head losses in all of the straight flow conduits are called "major," and a summation of all the components that change the velocity distribution (acceleration or deceleration of fluid particles), are called "minor." The minor loss occurs in laminar as well as turbulent flow. The summation of head losses is

$$\sum h = \sum_{major} f \frac{L}{D} \frac{V^2}{2} + \sum_{minor} K \frac{V^2}{2} \quad , \qquad (2)$$

where f is called the friction factor for each straight conduit of length L and diameter D, and K is a minor loss coefficient for each component (e.g., the bifurcations in the respiratory tract). For laminar fully developed flow f is analytically determined as

$$f = \frac{64}{\mathrm{Re}} \quad , \qquad (3)$$

where Re is the Reynolds number based on D and the density and viscosity of the fluid, ρ and η, respectively,

$$\mathrm{Re} = \frac{\rho V D}{\eta} \quad . \qquad (4)$$

After substituting Equations 2-4 into Equation 1 it can be shown that the major loss is independent of density for laminar flow. For turbulent pipe flow f has historically been determined empirically. For smooth tubes the correlation derived by Blasius can be used:

$$f = \frac{0.316}{\mathrm{Re}^{0.25}} \qquad (5)$$

The criterion used herein for differentiating laminar and turbulent flow was Re<2000. The minor loss coefficients for lung bifurcations were previously calculated based on computational fluid dynamics simulations.(8) In the present work the patient interface is broken into two components, the filter and the ETT and these minor loss coefficients

were determined through bench top experiments (13). Equation 1 was solved over a range of flow rates, for both inhalation and exhalation, and for each gas and ETT combination before fitting to equations of the form

$$\Delta p_{lung} = AQ^2 + BQ\,. \qquad (6)$$

For exhalation it is also necessary to calculate the pressure losses from the Y-piece of the breathing circuit through the ventilator, including the filter for carbon dioxide removal and the valve to produce positive end expiratory pressure (PEEP), back to the driving chamber for recirculation. An empirical relationship, excluding PEEP, based on major and minor losses was not employed because the precise flow path was not known.

$$\Delta p_{vent} = A\rho Q^2 + B\mu Q \qquad (7)$$

For pressure in units of N/m^2, Q in l/min, ρ in kg/m^3, μ in kg/s-m($x10^5$), A = 0.25 and B = 1. To account for PEEP the recorded value was simply added to the calculated pressure values. Property values at 1 atm and 37 °C for the gases used in the calculations are presented in Table 2.

Supine Morphology Model

The lungs are modeled as a symmetric, dichotomously branching network of stiff cylindrical tubes (the source of major losses) segmented into a series of bifurcating elements (the source of minor losses). The 23 generations (increasing incrementally from 0 at the trachea) are based on a morphology model for healthy adult male lungs; that is, mother and daughter diameters, length, and branching angle (θ = 70°) at each bifurcation are specified.(17) However, because airway resistance is greater in the supine position (18) the morphology model was modified by changing airway cross section shapes from circular to ellipsoid. The major and minor axes were taken to be 1.2D and 0.8D, respectively; then the hydraulic diameter used for calculations was $D_H \approx 0.94D$ based on a relation for elliptical cross sections (19). Thus in effect a smaller lung model was used to better represent the mixed gender and supine position of the subjects.

Numerical Integration

For inhalation, equation 6 was integrated in time using Excel (Microsoft, USA). At each new time step the alveolar pressure was calculated based on the compliance and volume at the previous time step, where the volume was calculated based on the imposed constant inhalation flow rate. For exhalation at each new time step equations 6 and 7 were solved for Q based on the alveolar pressure calculated using the lung compliance and volume from the previous time step.

Results

Examples of typical *in vivo* measurements, in this case taken for patient #9, in the form of individual symbols are shown in Figures 3-5; the panels are for 100% O_2, 30%/70% Xe/O_2, and 60%/40% Xe/O_2, respectively. For each of these figures panel A is the Y-piece pressure time trace and panel B is the flow rate (positive and negative values are for inhalation and exhalation, respectively) time trace. Superimposed on each graph are the

Table 2: Property values at 1 atm. and 37°C. (21)

Gas	Viscosity $x10^5$ (kg/s-m)	Density (kg/m^3)
Oxygen (O_2 100%)	2.113	1.257
Xenon (Xe/O_2 30/70%)	2.339	2.428
Xenon (Xe/O_2 60/40%)	2.395	3.599

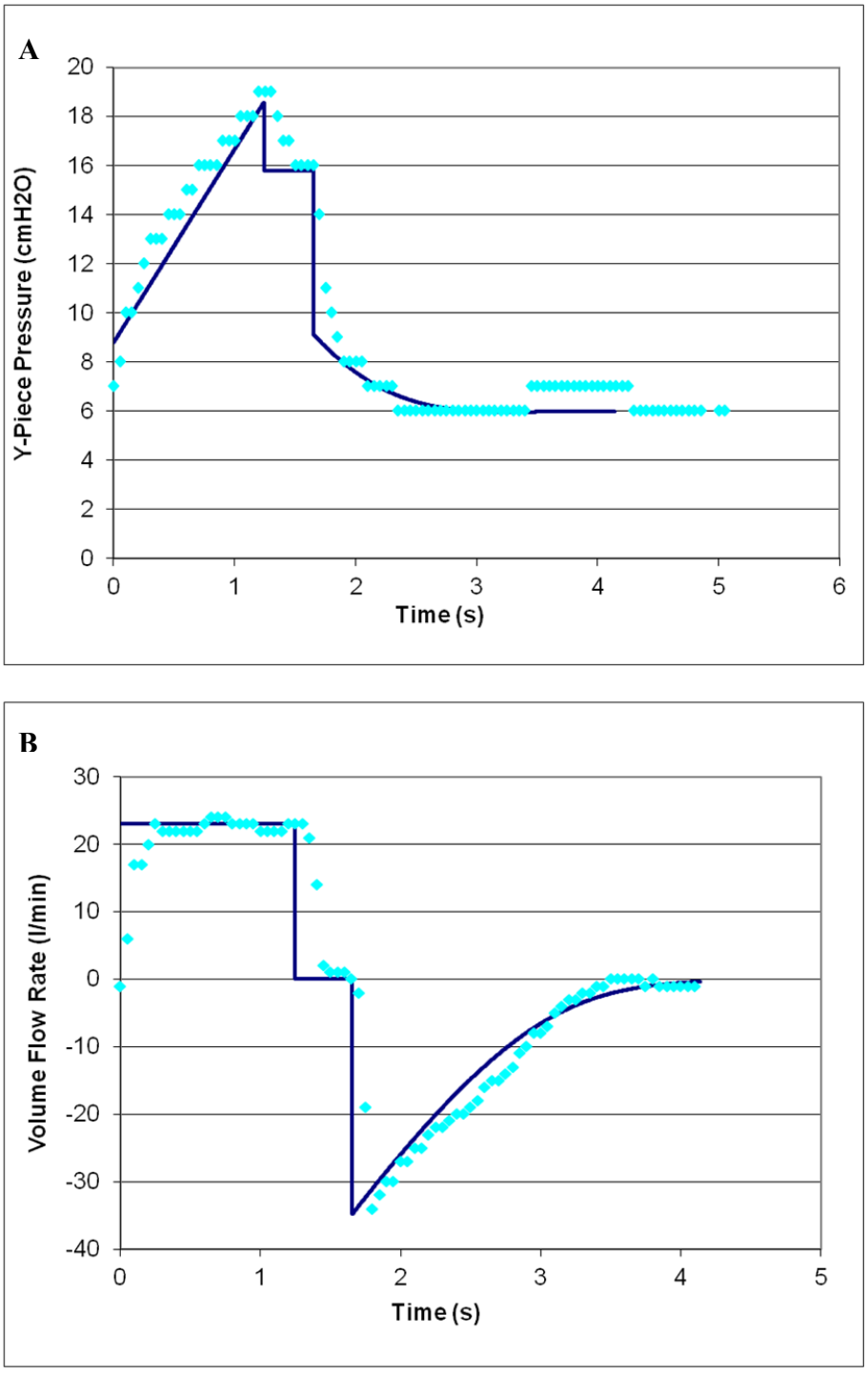

Figure 3: Panels A and B compare dynamic ventilatory parameters, Y-piece pressure and flow rate, respectively, for 100% O2, from experiments (individual symbols) and simulation (solid lines) for patient #9.

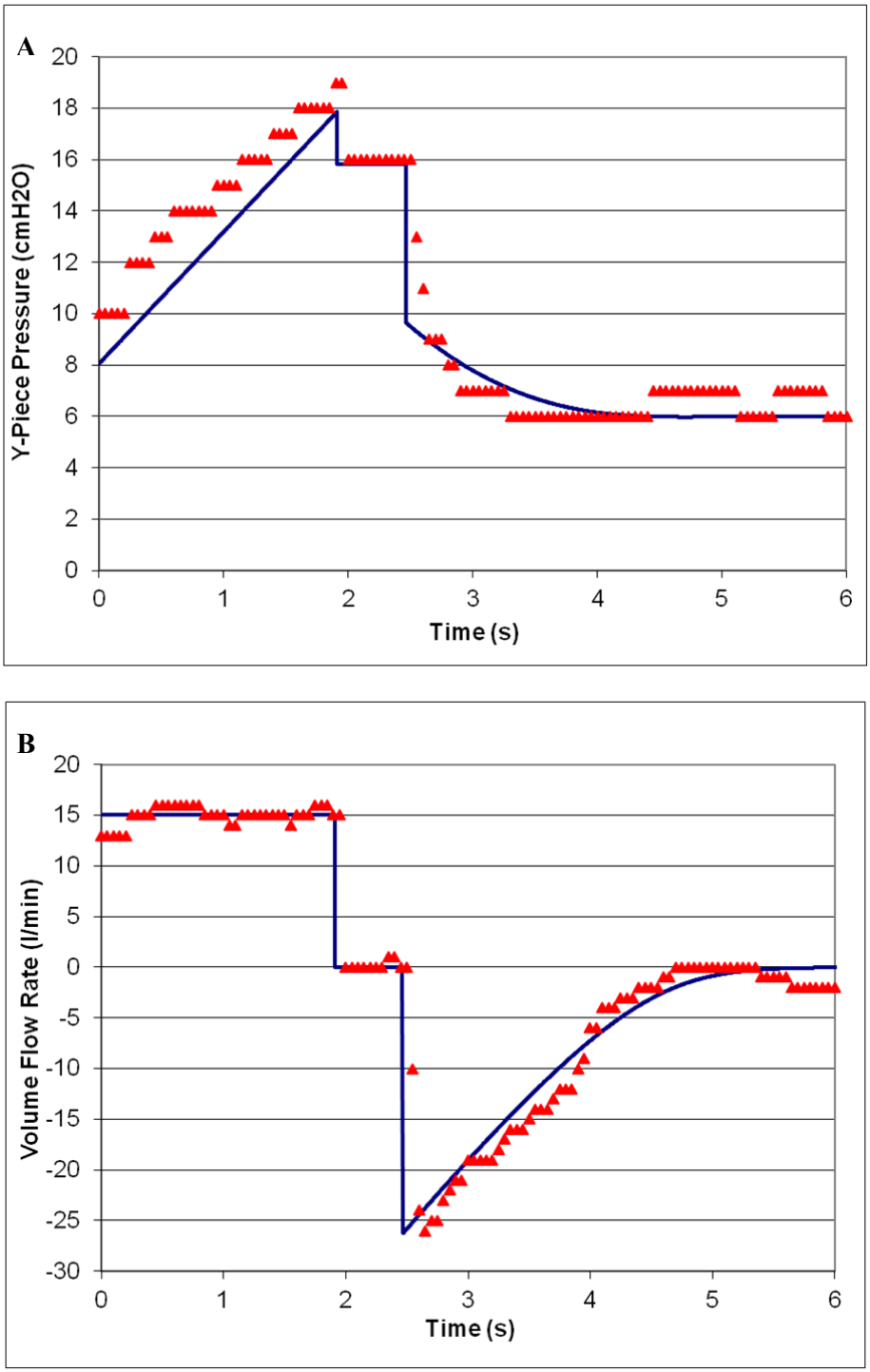

Figure 4: Panels A and B compare dynamic ventilatory parameters, Y-piece pressure and flow rate, respectively, for 30%/70% Xe/O2, from experiments (individual symbols) and simulation (solid lines) for patient #9.

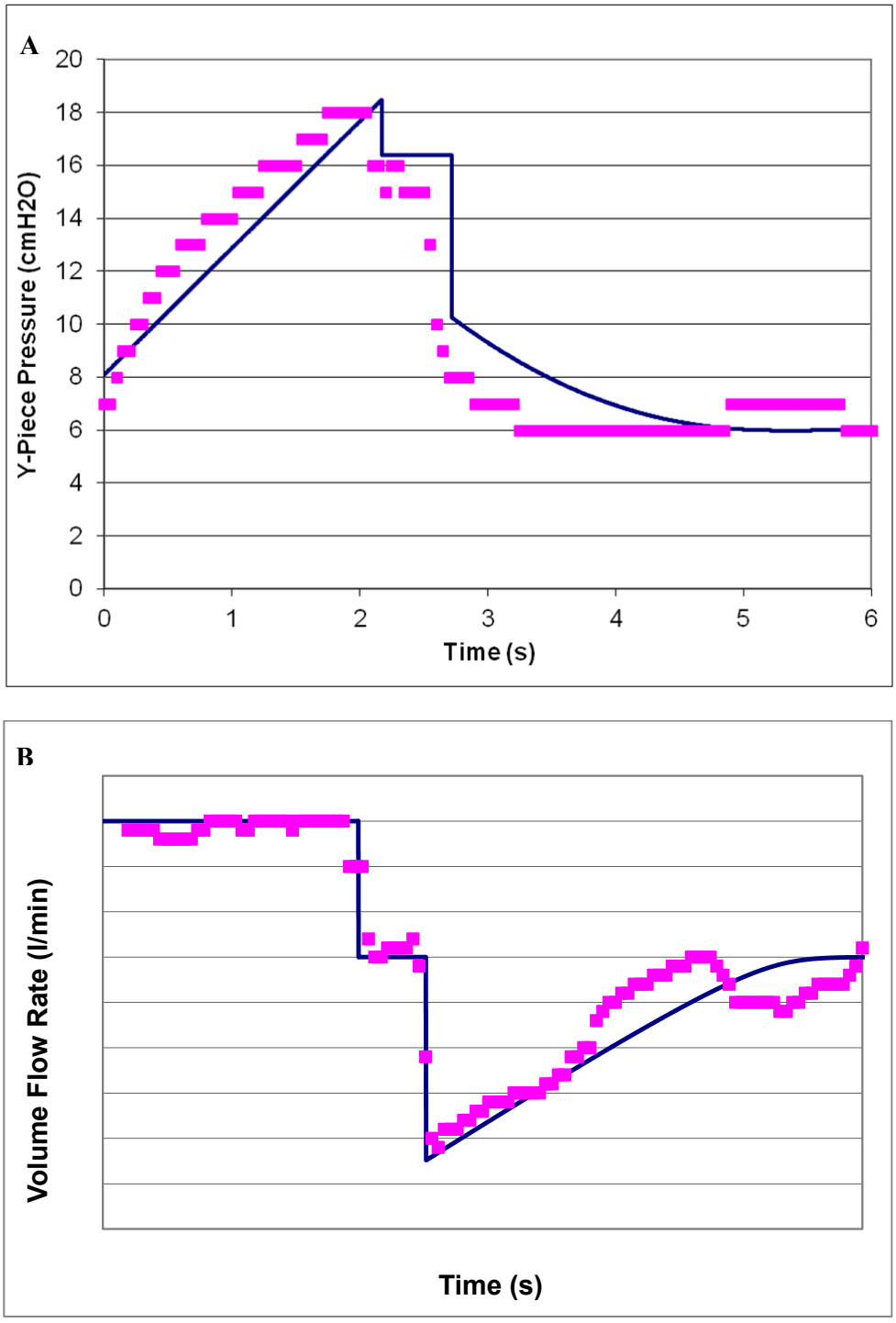

Figure 5: Panels A and B compare dynamic ventilatory parameters, Y-piece pressure and flow rate, respectively, for 60%/40% Xe/O2, from experiments (individual symbols) and simulation (solid lines) for patient #9.

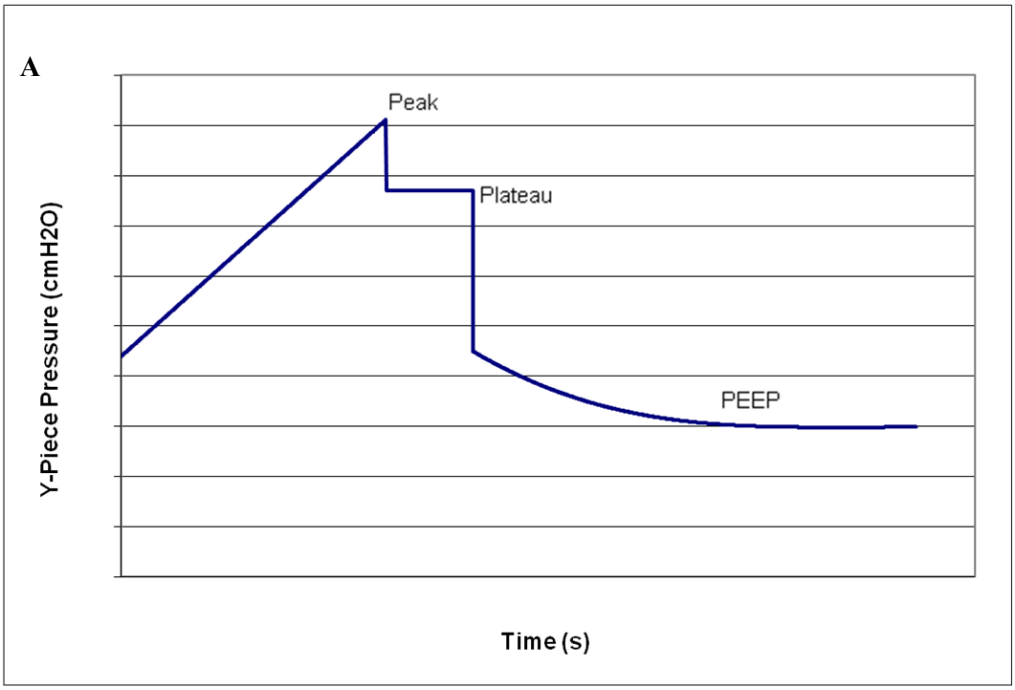

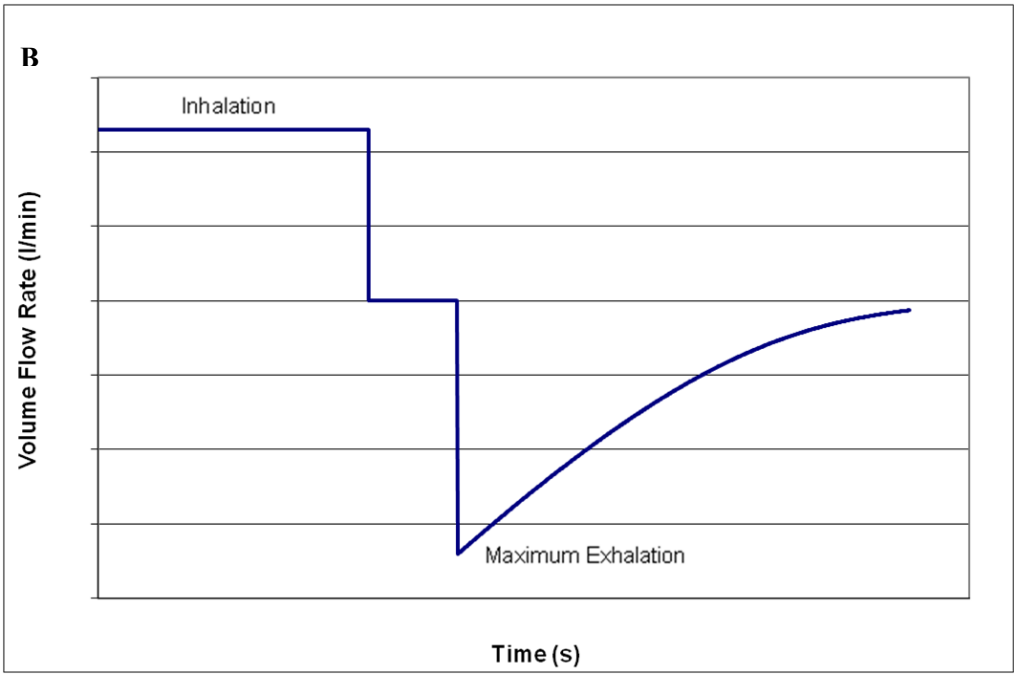

Figure 6: Characteristic pressure (Panel A) and flow rate (Panel B) curves indicating the specific parameters selected from the time series data used to compare experiments and simulations.

in silico results in the form of continuous lines based on the equivalent simulation. In Figure 6 key individual measurements that were drawn from each time series are defined. For inspiratory flow, where the ventilator maintains a constant flow rate during volume control mode, the key parameter is the peak-plateau pressure difference (panel A). For exhalation the maximum (negative) flow rate is used as the key parameter for comparison (panel B). Tables 3-5 compile the key information recorded and simulated for 100% O_2, 30%/70% Xe/O_2, and 60%/40% Xe/O_2, respectively, and for each patient; in principle this would be 30 individual experiments less the data that was unavailable or otherwise corrupted (3 cases). As noted in the previous section, the lung compliance for each patient was necessary to perform the simulation. The measured plateau-PEEP pressure difference, divided by the tidal volume was calculated for each experiment (Tables 3-5). The three values for each patient were then averaged (given in Table 1 with the standard deviation) and this value was used for the *in silico* simulations. Figure 7 shows a summary of the comparison of *in vivo* and *in silico* results for A) peak-plateau inhalation pressure difference and B) maximum expiratory flow rate. A comparison of inhalation airway resistance measured and calculated is given in Table 6.

Discussion

Presented herein are the *in silico* results in terms of ventilatory parameters of a numerical model compared to *in vivo* data collected during the wash-in phase of xenon anesthesia in patients without respiratory disease. The direct comparisons of model and experimental time histories of Y-piece pressure and flow rate shown in Figures 3-5 and the summarized comparisons in Figure 7 and Tables 3-6, indicate that with knowledge of the gas composition, ETT size, and lung compliance the dynamic ventilatory parameters can be predicted accurately.

The characteristic behavior in response to the gas mixtures is evident; that is, as density and viscosity increase the airway resistance increases, all else being equal. Moreover, the key ventilator parameters Y-piece pressure and maximum exhalation flow rate increase and decrease (in magnitude), respectively.

Figure 6 illustrates two unique parameters that are useful in quantifying the differences between theory and experiment, the peak-plateau pressure difference and the maximum exhalation flow rate. The peak-plateau pressure is a direct measure of the output of the engineering pressure loss model, direct because the inhalation flow rate is controlled by the ventilator to be constant. Exhalation is more complex because the driving force of the expanded lung is changing in time such that no single parameter can represent the total phenomenon. However, the maximum expiratory flow rate is easy to determine from the experimental and modeled data and reflects all of the physical mechanisms that influence exhalation. The slopes of the fitted data shown in Figure 7 are close to one indicating that overall there is a very good representation of the *in vivo* data by the *in silico* model (1.1252 and 1.0181, for the peak-plateau pressure and maximum exhalation flow rate, respectively). Table 6 compares measured and simulated inhalation airway resistance. The Pearson regression coefficient for the 27 resistance values measured and simulated is $r^2 = 0.8144$ determined using Excel (Microsoft, USA). The differences are predominantly caused by the uncertainty in pressure measurement as discussed below.

In spite of the overall accuracy of the simulations there are some inconsistencies between the *in vivo* and *in silico* results that originate from limitations of both the model and the experiments. It should be noted that results from patient #9 were presented because they are representative of the good correlation with the experimental measurements, but also because they typify the differences between measured and simulated re-

Table 3: Results from in vivo measurements and in silico simulations performed using 100% O2. No data was available for P#1.

100% O_2										
P#	**Qin (L/min)**	**TV (ml)**	**Compliance (ml/cm H2O)**	**Peak (cm H2O)**	**Plateau (cm H2O)**	**PEEP (cm H2O)**	**Ppeak-Pplateau (cm H2O)**	**Qexhal-max (l/min)**	**Simulated Ppeak-Pplateau (cm H2O)**	**Simulated Qexhal-max (l/min)**
1	No Data Available									
2	28	668	66.8	24	20	10	4	36	3.6	38.7
3	16	481	40.1	24	22	10	2	38	2.1	38.7
4	15	483	43.9	22	21	10	1	38	1.9	33.9
5	22	380	42.2	18	16	7	2	32	3.2	34.3
6	16	498	35.6	21	20	6	1	40	2.1	38.8
7	15	479	36.8	20	18	5	2	40	1.9	35.5
8	18	516	51.6	20	18	8	2	35	1.9	32.1
9	23	477	47.7	19	16	6	3	34	2.8	34.8
10	16	518	51.8	18	16	6	2	38	1.8	33.7

Table 4: Results from in vivo measurements and in silico simulations performed using 30%/70% Xe/O_2. No data was available for P#1.

30%/70% Xe/O_2										
P#	**Qin (L/min)**	**TV (ml)**	**Compliance (ml/cm H2O)**	**Peak (cm H2O)**	**Plateau (cm H2O)**	**PEEP (cm H2O)**	**Ppeak-Pplateau (cm H2O)**	**Qexhal-max (l/min)**	**Simulated Ppeak-Pplateau (cm H2O)**	**Simulated Qexhal-max (l/min)**
1	No Data Available									
2	19	624	52.0	24	22	10	2	26	2.9	27.8
3	16	489	37.6	27	23	10	4	33	2.8	29.2
4	15	483	43.9	24	21	10	3	26	2.6	25.6
5	13	404	40.4	20	17	7	3	24	2.1	26.8
6	15	524	43.7	21	18	6	3	26	2.6	29.9
7	15	494	44.9	20	17	6	3	28	2.6	27.2
8	15	545	60.6	19	17	8	2	20	2.1	25.1
9	15	478	47.8	19	16	6	3	26	2.1	26.2
10	17	514	46.7	20	17	6	3	26	2.4	25.3

Table 5: Results from in vivo measurements and in silico simulations performed using 60%/40% Xe/O_2. No data was available for P#3.

60%/40% Xe/O_2										
P#	**Qin (L/min)**	**TV (ml)**	**Compliance (ml/cm H2O)**	**Peak (cm H2O)**	**Plateau (cm H2O)**	**PEEP (cm H2O)**	**Ppeak-Pplateau (cm H2O)**	**Qexhal-max (l/min)**	**Simulated Ppeak-Pplateau (cm H2O)**	**Simulated Qexhal-max (l/min)**
1	18	551	50.1	27	21	10	6	32	4.2	22.8
2	19	643	53.6	27	22	10	5	28	3.4	23.7
3	No Data Available									
4	15	507	56.3	22	19	10	3	25	3.1	22.3
5	13	428	28.5	25	22	7	3	27	2.5	23.3
6	14	527	40.5	22	19	6	3	24	2.8	25.1
7	13	509	50.9	19	16	6	3	22	2.5	23.4
8	16	546	68.3	19	16	8	3	18	2.6	21.3
9	14	506	50.6	18	16	6	2	23	2.1	22.8
10	17	545	68.1	18	14	6	4	20	2.8	22.2

Table 6: Airway resistance. Standard deviations are in parenthesis. NA is not available.

	100% O_2			30%/70% Xe/O_2			60%/40% Xe/O_2		
P#	**R_{AW} Measured**	**R_{AW} Simulated**	**% Difference**	**R_{AW} Measured**	**R_{AW} Simulated**	**% Difference**	**R_{AW} Measured**	**R_{AW} Simulated**	**% Difference**
1	NA			NA			0.333	0.233	30.000
2	0.143	0.129	10.0	0.105	0.153	45.0	0.263	0.179	32.000
3	0.125	0.131	5.0	0.250	0.175	30.0	NA		
4	0.067	0.127	90.0	0.200	0.173	13.3	0.200	0.207	3.333
5	0.091	0.145	60.0	0.231	0.162	30.0	0.231	0.192	16.667
6	0.063	0.131	110.0	0.200	0.173	13.3	0.214	0.200	6.667
7	0.133	0.127	5.0	0.200	0.173	13.3	0.231	0.192	16.667
8	0.111	0.106	5.0	0.133	0.140	5.0	0.188	0.163	13.333
9	0.130	0.122	6.7	0.200	0.140	30.0	0.143	0.150	5.000
10	0.125	0.113	10.0	0.176	0.141	20.0	0.235	0.165	30.000
Avg	0.110(0.300)	0.126(0.011)	33.5	0.188(0.045)	0.159(0.016)	22.2	0.226(0.053)	0.187(0.026)	17.074

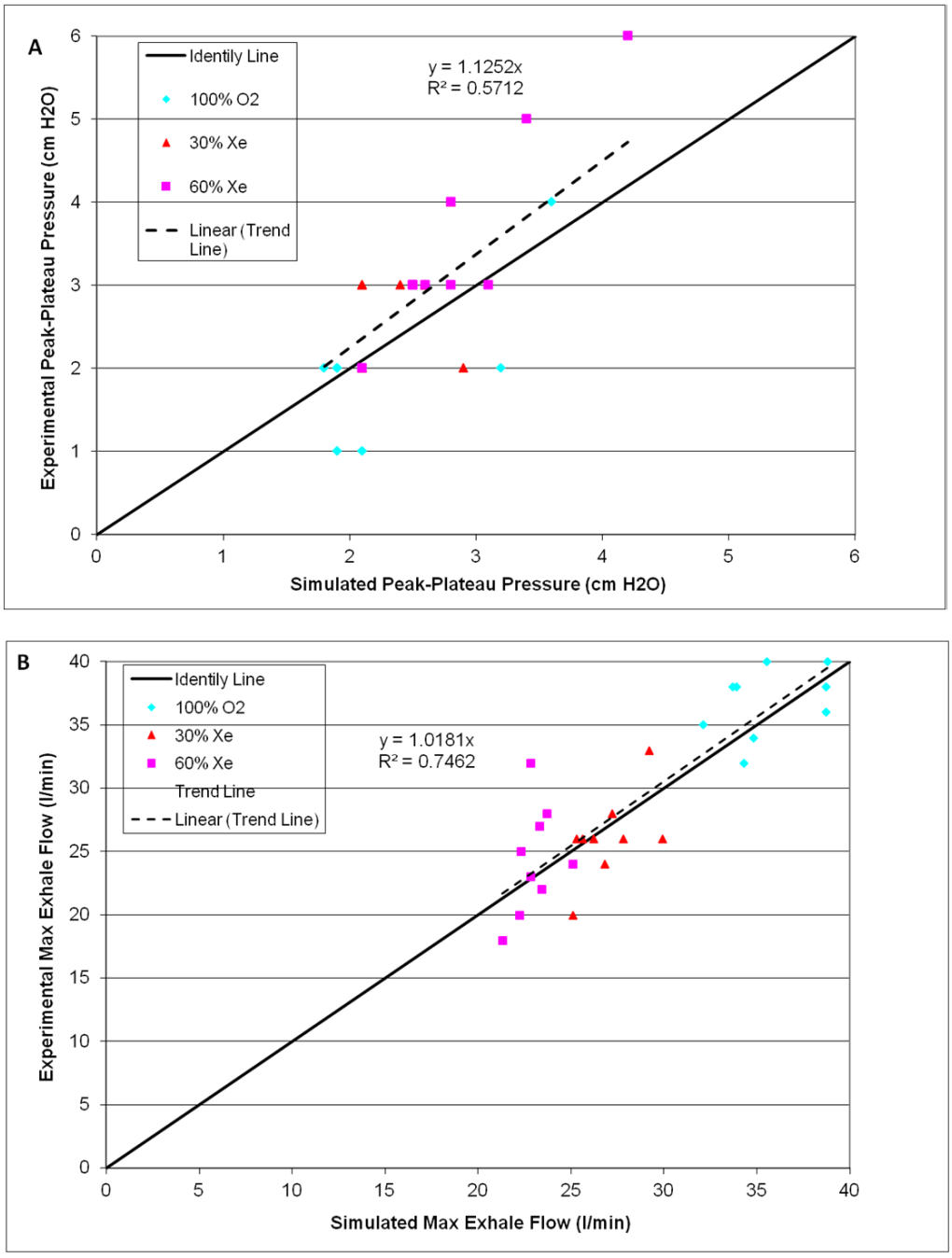

Figure 7: Comparisons of experimental and simulated: peak-plateau pressure (Panel A) and maximum exhalation flow rate (Panel B) for all the patients and all of the gases. The solid black line is the identity line indicating perfect agreement.

sults. Regarding the experiments, the low resolution of the reported data, especially for pressure, results in constant values over several time steps and the "stair step" distributions. This limitation is also a problem in knowing exactly when the breath was initiated which results in an offset of the inhalation Y-piece pressure curve in some cases (e.g., Figure 3A). Regarding the simulations, they assume idealized changes between ventilation phases; more precisely, that there is no mechanical inertia or friction in the system. This difference is evident at the start of exhalation. The simulated maximum exhalation always occurs at the first time step after the plateau is completed. In the experiments several time steps were required. Some of this lag could also be due to the time response of the data acquisition system. Certainly the key reason for differences with individual experiments is that the simulations are based on a single simplified morphology model. Considered of minor importance, the changes in fluid properties due to changes in gas concentration (i.e., carbon dioxide and water vapor) are assumed to be negligible. Furthermore, the engineering pressure loss model itself is also highly simplified compared to say a computational solution of the complete field equations for fluid mechanics.

The morphology model is generic, only accounting for the supine position. A similar model presented in Damanhuri et al. (6) was shown to be improved using a patient specific factor. The engineering pressure loss model used herein has only one path from the breathing circuit to the alveoli as a result of the symmetric morphology model employed, thus it was impossible to explore the role of heterogeneous resistance or compliance on ventilation. From previous studies on the effects of gas property variations on heterogeneous lung airway resistance (8,20), it is understood that for a normally compliant lung if the dominant mechanism of heterogeneous ventilation distribution is airway resistance then the lower the density and viscosity of the gas the more homogeneous the ventilation.

Conclusion

In this study *in silico* results were reported from the engineering pressure loss model for the human lung and shown to compare well to *in vivo* data recorded during the wash-in phase of xenon anesthesia. Based on these results the use of physics based models to inform physicians of the impact of administering gas mixtures seems feasible.

References

1. Otis AB, Fenn WO, Rahn H. Mechanics of breathing in man. J Appl Physiol. 1950; 2(11):592–607.
2. Borojeni AAT, Noga ML, Martin AR, Finlay WH. Validation of airway resistance models for predicting pressure loss through anatomically realistic conducting airway replicas of adults and children. J Biomech. 2015 Jul 16;48(10):1988–96.
3. Oppenheimer BW, Berger KI, Segal LN, Stabile A, Coles KD, Parikh M, et al. Airway dysfunction in obesity: response to voluntary restoration of end expiratory lung volume. PLOS One. 2014;9(2): e88015.
4. Kim K-H, Jahan SA, Kabir E. A review on human health perspective of air pollution with respect to allergies and asthma. Environ Int. 2013;59:41–52.
5. Condoluci C, Conte E, Angeletti G, Contu C, Fuso L. Correlation among functional respiratory parameters and disease control in asthma. Eur Respir J. 2015;46(suppl 59): PA5017.
6. Damanhuri NS, Docherty PD, Chiew YS, van Drunen EJ, Desaive T, Chase JG. A Patient-Specific Airway Branching Model for Mechanically Ventilated Patients. Comput Math Methods Med. 2014 Aug 20;2014: e645732.
7. Gattinoni L, Protti A, Caironi P, Carlesso E. Ventilator-induced lung injury: the anatomical and physiological framework. Crit Care Med. 2010;38(10):S539–48.

8. Katz IM, Martin AR, Muller P-A, Terzibachi K, Feng C-H, Caillibotte G, et al. The ventilation distribution of helium–oxygen mixtures and the role of inertial losses in the presence of heterogeneous airway obstructions. J Biomech. 2011;44(6):1137–43.
9. Pedley TJ, Schroter RC, Sudlow MF. The prediction of pressure drop and variation of resistance within the human bronchial airways. Respir Physiol. 1970;9(3):387–405.
10. Pedley TJ, Schroter RC, Sudlow MF. Energy losses and pressure drop in models of human airways. Respir Physiol. 1970;9(3):371–86.
11. Clark A, Rossmann JS, Katz IM, Martin AR, Caillibotte G. Pressure loss coefficients for asymmetric bifurcations of pulmonary airways with predetermined flow distributions. 2015 [cited 2016 Sep 1]; Available from: https://ldr.lafayette.edu/handle/10385/1944
12. Gemci T, Ponyavin V, Chen Y, Chen H, Collins R. Computational model of airflow in upper 17 generations of human respiratory tract. J Biomech. 2008;41(9):2047–54.
13. Katz IM, Martin AR, Feng C-H, Majoral C, Caillibotte G, Marx T, et al. Airway pressure distribution during xenon anesthesia: the insufflation phase at constant flow (volume controlled mode). Appl Cardiopulm Pathophysiol [Internet]. 2012 [cited 2016 Aug 30];16(5). Available from: http://www.applied-cardiopulmonary-pathophysiology.com/fileadmin/downloads/acp-2012-1_20120301/01_katz.pdf
14. Gouinaud L, Katz I, Martin A, Hazebroucq J, Texereau J, Caillibotte G. Inhalation pressure distributions for medical gas mixtures calculated in an infant airway morphology model. Comput Methods Biomech Biomed Engin. 2015 Sep 10;18(12):1358–66.
15. Stoppe C, Fahlenkamp AV, Rex S, Veeck NC, Gozdowsky SC, Schälte G, et al. Feasibility and safety of xenon compared with sevoflurane anaesthesia in coronary surgical patients: a randomized controlled pilot study. Br J Anaesth. 2013 Apr 11;aet072.
16. Stoppe C, Rimek A, Rossaint R, Rex S, Stevanovic A, Schälte G, et al. Xenon consumption during general surgery: a retrospective observational study. Med Gas Res. 2013 Jun 11;3:12.
17. Soong TT, Nicolaides Py, Yu CP, Soong SC. A statistical description of the human tracheobronchial tree geometry. Respir Physiol. 1979;37(2):161–72.
18. Attinger EO, Monroe RG, Segal MS. The mechanics of breathing in different body positions. I. In normal subjects. J Clin Invest. 1956;35(8):904.
19. Shaughnessy EJ, Katz IM, Schaffer JP. Introduction to fluid mechanics [Internet]. Oxford University Press New York; 2005 [cited 2016 Aug 30]. Available from: http://www.academia.edu/download/43976514/Introduction_to_Fluid_Mechanics.pdf
20. Martin AR, Katz IM, Terzibachi K, Gouinaud L, Caillibotte G, Texereau J. Bench and mathematical modeling of the effects of breathing a helium/oxygen mixture on expiratory time constants in the presence of heterogeneous airway obstructions. Biomed Eng Online. 2012;11(1):1.
21. Katz I, Caillibotte G, Martin AR, Arpentinier P. Property value estimation for inhaled therapeutic binary gas mixtures: He, Xe, N2O, and N2 with O2. Med Gas Res. 2011;1(1):1.

Ira Katz
Medical R&D
Centre de Recherche Claude-Delorme
1 chemin de la Porte des Loges
Les Loges-en-Josas, B.P. 126
78354 Jouy-en-Josas Cedex
France
ira.katz@airliquide.com